



ELSEVIER

Available online at www.sciencedirect.com

SCIENCE @ DIRECT®

Journal of Sound and Vibration 283 (2005) 821–851

JOURNAL OF
SOUND AND
VIBRATION

www.elsevier.com/locate/jsvi

Helicopter rotor blade frequency evolution with damage growth and signal processing

Niranjan Roy, Ranjan Ganguli*

Department of Aerospace Engineering, Indian Institute of Science, Bangalore 560012, India

Received 21 November 2003; received in revised form 7 May 2004; accepted 17 May 2004

Available online 5 November 2004

Abstract

Structural damage in materials evolves over time due to growth of fatigue cracks in homogenous materials and a complicated process of matrix cracking, delamination, fiber breakage and fiber matrix debonding in composite materials. In this study, a finite element model of the helicopter rotor blade is used to analyze the effect of damage growth on the modal frequencies in a qualitative manner. Phenomenological models of material degradation for homogenous and composite materials are used. Results show that damage can be detected by monitoring changes in lower as well as higher mode flap (out-of-plane bending), lag (in-plane bending) and torsion rotating frequencies, especially for composite materials where the onset of the last stage of damage of fiber breakage is most critical. Curve fits are also proposed for mathematical modeling of the relationship between rotating frequencies and cycles. Finally, since operational data are noisy and also contaminated with outliers, denoising algorithms based on recursive median filters and radial basis function neural networks and wavelets are studied and compared with a moving average filter using simulated data for improved health-monitoring application. A novel recursive median filter is designed using integer programming through genetic algorithm and is found to have comparable performance to neural networks with much less complexity and is better than wavelet denoising for outlier removal. This filter is proposed as a tool for denoising time series of damage indicators.

© 2004 Elsevier Ltd. All rights reserved.

*Corresponding author. Tel.: +91-080-3942438; fax: +91-080-3600134.

E-mail addresses: niranjan@aero.iisc.ernet.in (N. Roy), ganguli@aero.iisc.ernet.in (R. Ganguli).

Nomenclature			
		m_0	mass per unit length of blade
		Ω	rotation speed, scalar quantity
EI_y	flap-bending stiffness	R	rotor radius
EI_y	lag bending stiffness	U	strain energy
GJ	torsion stiffness	T	kinetic energy

1. Introduction and background

Helicopters are susceptible to damage in the main and tail rotor blades and in the transmission system due to gear spalling. A helicopter main rotor system operates in a severe dynamic and unsteady aerodynamic environment leading to fatigue damage. Therefore, helicopter rotor blades require frequent inspection, repair and replacement. The rotor blade in a helicopter is a highly sensitive part because it is exposed to periodic vibratory and fatigue loads as well as the threat of ballistic damage. Several researchers have addressed the damage detection and isolation problem for helicopter blades in recent years using helicopter rotor response and hub loads [1–4]. In general, these studies were conducted using mathematical models of the damaged rotor in flight. However, hub loads are difficult to measure in flight. Addressing this issue, Kiddy and Pines [5] detected damage in rotating composite beams using a constrained minimization of the modal residuals of the structural response. Cattarius and Inman [6] used beat phenomenon approach to detect structural damage in helicopter rotor blade. The authors in Ref. [6] also modeled the damage a mass increase (locally added weight) and mass decrease (drilled holes in the structure). The beat phenomenon is derived from frequencies but magnifies changes in frequencies due to damage. Ganguli [7] developed a fuzzy logic-based algorithm based on both non-rotating and rotating frequencies and showed that damage could be detected using rotor blade modal data. In general, the damage detection in helicopter blades is based on some health measure of the system. Typical health measures are changes in blade flap (out-of-plane bending), lag (in-plane bending) and torsion deflection between damaged and undamaged blades, vibratory hub loads, fuselage vibration, blade frequencies and mode shapes.

Modal frequencies are often poor indicators of incipient damage because they are the global properties of the system and exhibit small changes even for large damage levels. However, according to Cattarius and Inman [6], helicopter blades are designed to take substantial amount of damage prior to failure. Because helicopter blades are designed to sustain considerable damage [7], the use of rotating frequencies for online health monitoring appears useful. Larsen et al. [8] used modal parameters to monitor damage in wind turbines. Larsen et al. [8] note that small damages do not affect modal properties to a measurable extent. Therefore, the modal damage indicator acts as a filter which avoids false alarms due to insignificant damage.

Recent studies have looked at online estimation of frequencies [9,10]. Rew et al. [9] investigated various methods for the real-time estimation of multi-modal frequencies and validated through numerical results using experimental tests. Brinker et al. [9] introduced a new frequency domain technique for the modal identification of output-only systems, i.e. in the case where the modal parameters must be estimated without knowing the input exciting the system. The technique

introduced by Brinker et al. [10] is user friendly and is closely related to the classical approach where the modal parameters are estimated by simple peak picking.

Selected studies have looked at application of experimental modal testing to rotating structures [11]. Wilkie et al. [12] conducted a modal analysis of a model helicopter blade in a hover test facility. Rotating frequency measurements for each mode were made at rotor speeds that ranged from 150 to 660 rpm at approximately 100 rpm intervals; the non-oscillating collective pitch of the blades was fixed at 0° . At each rpm considered, the blades were excited by sinusoidally exciting the collective pitch of the rotor with a hydraulic control system. The collective pitch oscillation frequency was varied over a 10–20 Hz frequency band in the vicinity of each modal frequency. The amplitude of the vibrating hub loads caused by swash plate movement together with the small amount of aerodynamic excitation due to collective pitch oscillation was sufficient to excite all the modes present. The blade modal frequencies were obtained by processing blade and pitch link strain gauge signals with an electronic signal analyzer. Output signal from the strain gauges mounted on the blade were used as a measure of the blade modal deflection. The pitch-link mounted strain gauge signals were used as a measure of the force input to the structure. A signal analyzer was then used to generate a frequency response function from these measurements. The frequency of the excited blade mode was obtained from the amplitude peak of the frequency response function. A schematic representation of this is given in Fig. 1.

Most rotor health-monitoring work has looked at diagnostics, which involves static indicators, where as prognostics involves dynamic indicators. Diagnostics indicates whether or not damage has taken place and provides indication about the severity of damage. Prognosis indicates the rate at which damage is accumulating and the remaining useful life that could be expected from a component or system. Some researchers have started looking at prognostics using a dynamical systems approach [13,14]. These approaches consider a slowly evolving damage process coupled to a directly observable fast-time dynamical system. These algorithms are not related to any specific damage physics and are general in nature.

Physically, it is clear that fatigue damage growth is an important aspect of the evolution of damage in helicopter rotor blades. While the fatigue of homogenous materials is well understood, the analysis of fatigue in composites is difficult because the material properties of the constituents of the composite are quite different. For homogenous materials, damage accumulates at a slow rate in the beginning and a single crack propagates in a direction perpendicular to the cyclic loading axis. Fatigue damage in homogenous materials increases with applied cycles in a

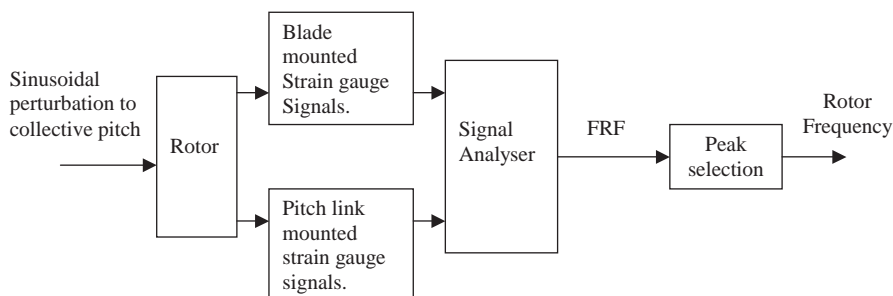


Fig. 1. Schematic representation of rotating frequency measurement.

cumulative manner [15]. On the basis of damage curve concept, this damage can be represented by a power relationship $D = (n/N)^{m_1}$, which is the nonlinear load-dependent damage theory [15]. Therefore, damage accumulation in homogenous material as shown in Fig. 2 can be mathematically modeled using

$$D = \left(\frac{n}{N}\right)^{m_1} \quad (1)$$

where D is the normalized accumulated damage, m_1 is a material-dependant parameter, n is the number of applied loading cycles, and N is the fatigue life at the corresponding applied load level. However, in composite materials, the fracture behavior is characterized by multiple damage modes like crazing and cracking of the matrix, fiber/matrix decohesion, fiber fracture, ply cracking, delamination void growth, and multidimensional cracking. All these modes occur early in the fatigue life of composites.

The mechanics of crack initiation and crack growth are very complicated in composite materials. Even for simple tension loading of a unidirectional reinforced composite along the fiber direction, cracks can initiate at different locations and in different directions. Crack can initiate in the matrix, perpendicular to the direction of loading. Cracks can also initiate at the interface between the fiber and the matrix in the direction of the fibers due to debonding. For general composite laminates, fracture mechanics cannot be used for fatigue analysis of composite materials.

Fiber reinforced composites are good for fatigue life. However, the same does not apply to the number of cycles to initial damage or to the evolution of damage. In a recent paper, Degrieck and Paepegem [16] have classified fatigue models based on these basic categories. The first one approach does not take into account the actual degradation approaches, but uses S–N curves and introduces some sort of fatigue failure criterion. These so-called fatigue life models are developed by extensive experimental work. The second class of models includes the phenomenological models for residual stiffness and strength. Residual stiffness models account for the degradation of elastic properties during fatigue. Stiffness can be measured frequently during fatigue experiments and can be measured without further degrading the materials. Some models are deterministic and a single-valued stiffness property is predicted. Others are statistical and predict stiffness distributions. The third class of models describe the deterioration in the composite

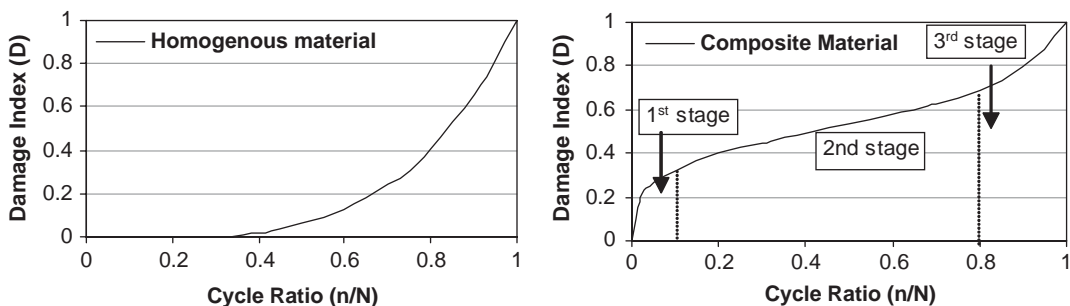


Fig. 2. Damage accumulation with cycle ratio.

material in direct relation to the actual physical damage such as transverse matrix cracks, delamination size, etc. These models are also called mechanistic models. Mechanistic models are difficult to apply because fatigue damage growth is complex in terms of evolution and geometry. Some mechanistic models consider as many as seven difficult damage mechanisms. However, the application of such models is a cumbersome task and needs finite element analysis of the individual matrix and stresses.

The modulus decay due to fatigue in composite material can be divided into three stages [16]. Stage I undergoes a rapid stiffness reduction. This reduction is mostly due to the development of transverse matrix cracks. Stage II damage growth occurs in an almost linear fashion with respect to cycles and accounts for the high fatigue life of composites. This stage is dominated by edge delamination and additional longitudinal cracks along the 0° fibers. Stage III shows rapid stiffness degradation purely due to local damage progression and the initial fiber fractures leading to strand failures.

The stiffness-based models can be defined in terms of a damage variable D where $D = 1 - E/E_0$. Here D is the accumulated fatigue damage, E_0 is the Young's modulus of the undamaged material, and E is the Young's modulus of the damaged material. The extent of damage is thus quantified by measuring the Young's modulus of the material. Early damage models included a linear damage accumulation model by Nicholas and Russ [17]. Other nonlinear damage accumulation functions here have also been used [18,19]. These early models could not effectively capture all the three damage stages. For example, the model proposed by Subramanian [18] explains the fast damage growth during the early loading cycles in stage I but does not properly describe the rapid damage growth in stage III. Halverson et al. [19] models the stage III quite well but not the stage I. Mao and Mahadevan [20] have recently proposed a mathematical model that accurately describes all three stages of the damaged process. They proposed a function of the form

$$D = q\left(\frac{n}{N}\right)^{m_1} + (1 - q)\left(\frac{n}{N}\right)^{m_2}. \quad (2)$$

Here D is the normalized accumulated damage, q , m_1 and m_2 are parameters, n is the number of applied cycles, N is the fatigue life at the corresponding applied load level. The first term in the above equation with $m_1 < 1$ captures the rapid damage accumulation during stage I. The second term shows the fast damage growth at the end of the fatigue life with that at the end of the fatigue life with $m_2 > 1$. The parameters q , m_1 and m_2 are obtained from fatigue experiments. The nature of the damage curves for homogenous and composite materials is shown in Fig. 2.

It is possible to measure the stiffness degradation directly in test specimens. However, in realistic structures it is easier to measure or track another variable which is tied to the stiffness. Moon et al. [21] propose the use of natural frequencies of composite laminates as a global damage variable. The fatigue damage state of the structure can then be measured using the so-called 'residual natural frequency' which could be measured from vibration tests. The authors demonstrate experimentally that enough frequency degradation can be obtained to monitor the condition of composite laminates.

Badewi and Kung [22] also studied the effect of fatigue on the modal properties of composite structures. They correlated their results in changes in modal properties to select graphite epoxy composite specimen. They mention that the idea of using modal properties can be used as a real time indicator of damage in structures. The authors also mention that nondestructive methods

such as those based on C-scan, thermography, acoustic emission and others have been demonstrated to various extents for detecting internal damage in composites. A shortcoming of these approaches is the need for sophisticated equipment and highly skilled operators. Further, the interpretation of the output from these devices is not straightforward.

Older helicopter rotors were often made of aluminum, while newer rotors are fabricated using composite materials. Composite materials are widely used in numerous aerospace applications because of their high specific stiffness to weight ratio and strength. Fatigue is the main failure mechanism for structures under cyclic loading. Helicopter rotors are subject to 1/rev loads as the primary source of fatigue. This fatigue mechanism is due to the time-varying velocity experienced by the blade section in forward flight, which leads to time-varying aerodynamic forces. In this study, we investigate the behavior of typical rotor system damage indicators such as blade-rotating frequencies of the damaged blade. The results are qualitative as we are concerned about the functional nature of evolution of rotor system parameters with fatigue damage growth, and not with their exact values, which can be changed for different structures because of the nature of loading, characteristic of the composite laminate and inherently stochastic nature of damage growth. The results in this study provide insight into how the values of the rotor system modal parameters evolve with time and compare the difference between rotors made of composite materials with those made of homogenous materials. The results also show if fatigue damage causes enough changes in the rotating frequencies to be measurable, given the considerable stiffening effect of rotation. Further, the simulated data generated using the finite element simulations are used to study signal-processing algorithms for use in improved health monitoring. Because operational rotor data are noisy and have outliers, signal processing prior to the use of data for diagnostic and prognostics is very useful. A powerful recursive median filter and radial basis neural network and wavelet-based approach are developed and compared for denoising the rotor frequency signals.

2. Finite element model of helicopter rotor blade

The helicopter blade is modeled as an elastic beam undergoing flap (transverse) bending, lag (in-plane) bending, elastic twist and axial deflections [23]. Governing equations for free vibration of a rotor blade are derived using Hamilton's principle over a time period of rotor revolution ($\psi = 0 - 2\pi$):

$$\delta\Pi = \int_0^{2\pi} (\delta U - \delta T) d\psi = 0, \quad (3)$$

where δU and δT are virtual variations of strain energy and kinetic energy respectively and $\delta\Pi$ represents the total potential of the system. The δU and δT are based on the Hodges and Dowell [23] approach and are given in Ref. [24].

Finite element methodology is used to discretize the governing equations of motion. After discretization, the Hamilton's principle can be written as

$$\int_0^{2\pi} \sum_{i=1}^N (\delta U_i - \delta T_i) d\psi = 0. \quad (4)$$

The blade is discretized into N finite beam elements of equal length. Each beam element consists of 15 degrees of freedom as shown in Fig. 3 with $N=20$. These degrees of freedom correspond to cubic variations in axial elastic and (flap and lag) bending deflections and quadratic variation in elastic torsion (Nomenclature). Element connectivity is established by continuity of slope and displacement for transverse and inplane bending deflections, whereas for elastic twist and axial deflection it is established by continuity of displacements. Such an element ensures linear variations of bending and torsion moments and quadratic variation of axial force within the elements. These degrees of freedom are distributed over five element nodes (two boundary and three interior nodes). There are six degrees of freedom at each element boundary node. These six degrees of freedom correspond to u_e, v, v', w, w' and $\hat{\phi}$. There are two internal nodes for axial deflection u_e , and one internal node for elastic twist $\hat{\phi}$. Between elements there is continuity of displacement and slope for flap and lag bending deflections, and continuity of displacement for elastic twist and axial deflections. The two internal nodes are needed for the axial degree of freedom to accurately represent the distribution of centrifugal force over the element. With two internal nodes, the distribution of u_e over the element is cubic. Hence, the axial force distribution is quadratic and of the same order as the centrifugal force. The internal node for the torsional deflection assumes that the torque approximation over the element is of the same order as the flap and lag bending moment [25].

Using interpolation polynomials, the distribution of deflection over a beam element is expressed in terms of the elemental nodal displacements q_i . For the i th beam element, one would obtain the

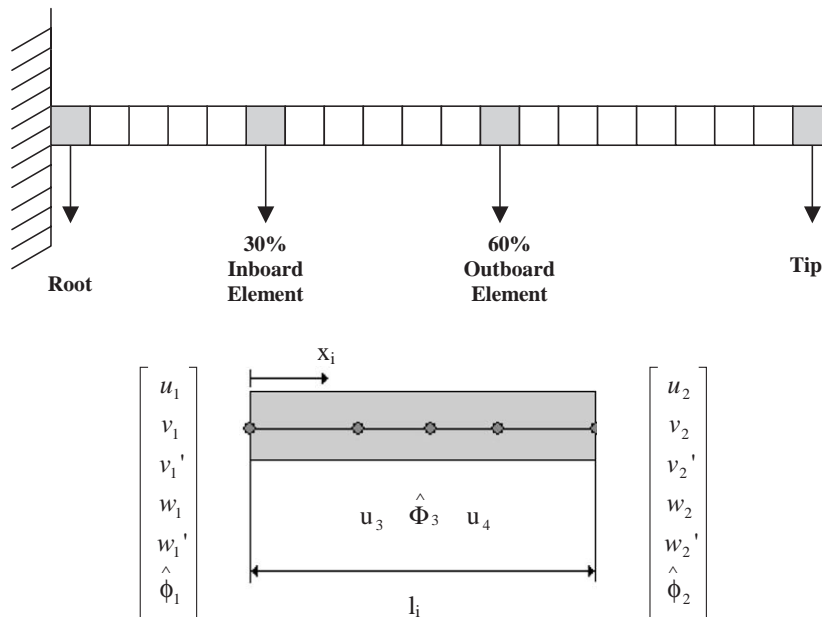


Fig. 3. Rotor blade finite element model and locations of simulated structural damage (20 elements of equal length).

blade deflections as

$$u(s) = \begin{Bmatrix} u(s) \\ v(s) \\ w(s) \\ \hat{\phi}(s) \end{Bmatrix} = \begin{bmatrix} \mathbf{H}_u & 0 & 0 & 0 \\ 0 & \mathbf{H} & 0 & 0 \\ 0 & 0 & \mathbf{H} & 0 \\ 0 & 0 & 0 & \mathbf{H}_{\hat{\phi}} \end{bmatrix} q_i, \quad (5)$$

where the elemental nodal displacement vector is defined as

$$\mathbf{q}_i^T = [u_1 \quad u_2 \quad u_3 \quad u_4 \quad v_1 \quad v'_1 \quad v_2 \quad v'_2 \quad w_1 \quad w'_1 \quad w_2 \quad w'_2 \quad \hat{\phi}_1 \quad \hat{\phi}_2 \quad \hat{\phi}_3] \quad (6)$$

For frequency analysis, the elemental mass and stiffness matrices are derived and then assembled to form the global mass and stiffness matrix. The cantilever boundary conditions are then applied to the global mass and stiffness matrix. The rotating frequencies of the helicopter blade are then calculated.

3. Damage modeling

Damage is modeled using the concept of effective stress. Thus, for undamaged material $\varepsilon = \sigma/E$ and for damaged material $\varepsilon = \sigma/E(1 - D)$. The elasticity modulus of the damaged material is defined as [26]

$$E^{(d)} = E^{(u)}(1 - D), \quad (7)$$

where the superscripts u and d represent the undamaged and the damaged state of the structure. With this model, $D = 0$ corresponds to no damage and $D = 1$ to complete damage. The experimental results for composite materials show that the measured Young's modulus or stiffness just before complete failure of the specimen is not zero. The final accumulated damage is $1 - E_f/E^{(u)}$ instead of unity when the material fails, where E_f is the Young's modulus when the material fails. Therefore, for composite materials, a new damage parameter can be defined with the final Young's modulus E_f as

$$D = \frac{E^{(u)} - E^{(d)}}{E^{(u)} - E_f}. \quad (8)$$

We can calculate the damage of the material using either of the parameters described with Eqs. (7) or (8) depending on whether the material is homogenous or heterogeneous. Because here we are doing a qualitative study of the effect of the damage growth on rotor system parameters, we assume $E_f = 0$, so for our convenience we use the damage parameter described with Eq. (7). The plots in Fig. 2 are taken from Ref. [20] and are used to model the evolution of damage in the material. We assume a constant applied load in this study.

4. Background on signal processing

We show later in the paper that modal frequencies can be used to monitor the growth of damage. However, operational data from a helicopter rotor are noisy and contaminated with

outliers. Linear filters are not good at removing outliers. Therefore, we study three nonlinear filters: (1) weighted recursive median filter (WRM), (2) radial basis function (RBF) neural networks and (3) wavelets to denoise the simulated signals and compare the results with a linear finite impulse response (FIR) moving average filter. The application of the WRM Filter in damage detection is new in this study.

4.1. Weighted recursive median filter

Recursive median (RM) filters are an important class of nonlinear filters. Recursive median filters possess superior noise attenuation capability than their non-recursive counterparts [27]. A RM filter uses some previous output values, instead of the input values for arriving at the next output i.e. for a RM filter

$$y_n = \text{median}(y_{n-k}, y_{n-k+1}, \dots, x_n, \dots, x_{n+k-1}, x_{n+k}), \quad (9)$$

where $N = 2k + 1$ is the window length of the filter. Recursive median filters also have a higher immunity to impulsive noise or outliers in the data than median filters. With the same number of operations, recursive filters achieve more noise reduction than non-recursive filters.

A modified version of the recursive median filters is the WRM filter [28]. The weights allow the filter to be tuned to particular types of signals.

$$y_n = \text{median}(w_{n-k} \circ y_{n-k}, w_{n-k+1} \circ y_{n-k+1}, \dots, w_n \circ x_n, \dots, w_{n+k-1} \circ x_{n+k-1}, w_{n+k} \circ x_{n+k}), \quad (10)$$

where $N = 2k + 1$ is the window length of the filter and \circ stands for duplication. While weights can take on real values, it has been proved that integer values are adequate for a weighted median filter. Filters with positive integer weights are limited to low-pass capabilities. In our damage detection applications, we are looking at a ‘low-pass’ application where a health residual is contaminated with high-frequency Gaussian noise and outliers. Hence we shall only consider positive integer weights. The weights can be chosen to be symmetric, $w_{n-i} = w_{n+i}$, $i = 0, 1, 2, \dots, k$ to avoid bias effects [29]. Problems where an infinite number of iterations are needed by a weighted median filter can often be synthesized by a single pass of a properly designed recursive weighted median filter. WRM filter can achieve the effects of non-recursive WM filter of much longer window sizes. The calculation of proper weights is important for such filters and allows their tuning for specific type of signals. This weight selection is considered later in this study.

4.2. RBF neural network

Multilayer perceptron neural networks trained using back propagation have been used in denoising signals [30,31]. However, these networks are very time consuming for training. An alternative approach using the radial basis function network (RBFN) is used in this study. The RBFN model consists of three layers: an input layer, a hidden (kernel) layer and an output layer. The nodes within each layer are fully connected to the previous layer. The input variables are each assigned to a node in an input layer and pass directly to the hidden layer without weights. The hidden nodes or units contain the RBF, also called transfer functions. An RBF is symmetrical about a given mean or center point in a multidimensional space. In the RBFN, a number of

hidden nodes with RBF activation functions are connected in a feed-forward parallel architecture. The parameters associated with the RBFs are optimized during training. The *K*-means clustering approach [32] is used to train the RBFN. Details of this approach are given by Leonard [32] and by Reddy and Ganguli [24].

4.3. Wavelet

Wavelets can also be used for denoising signals. The wavelet transform (WT) was developed as a method to obtain simultaneous, high-resolution time and frequency information about a signal by using a variable-sized window region (the wavelet) instead of a constant window size. Because the wavelet may be dilated or compressed, different features of the signal are extracted. A narrow wavelet picks up on the lower frequency components of the signal. The mathematical description of the continuous wavelet transform (CWT) is described by

$$\text{CWT}_x^\psi(\tau, s) = \Psi_x^\psi(\tau, x) = \frac{1}{\sqrt{|s|}} \int x(t) \psi^*\left(\frac{t-\tau}{s}\right) dt. \quad (11)$$

The scale, s , of the wavelet may conceptually be considered as the inverse of frequency. The wavelet is compressed if the scale is low and dilated if the scale is high. The CWT reveals more details about a signal, but because all scales are used to compute the WT, the computation time required can be enormous. Therefore, the discrete wavelet transform (DWT) is normally used. The DWT calculates the wavelet coefficients at discrete intervals of time and scale, instead of at all scales. The DWT requires much less computation than the CWT without much loss in detail. With the DWT, a fast algorithm is possible which possesses the same accuracy as other methods. The algorithm makes use of the fact that if scales and positions are chosen based on powers of two (dyadic scales and positions) the analysis is very efficient. More details about wavelets are available from Ref. [33].

5. Numerical simulations

We consider a uniform equivalent to a Eurocopter BO105 hingeless helicopter rotor blade and add damage in the blade at different locations of the blade. Rotor properties are shown in Table 1 and are taken from Ref. [34]. The blade is divided into 20 finite elements of equal length. The frequencies of the baseline rotor are shown in Table 2, where they are non-dimensionalized using rotor speed. The locations of damage are at the root, an inboard element which is at 30% of blade radius from the rotor and an outboard element that is 60% from the root. The frequencies considered are the first four flap and lag frequencies and the first two torsional frequencies. Using the damage curves shown in Fig. 2, least-square method can be used to optimize the values of the parameters of Eqs. (1) and (2). The damage growth curve for homogenous material shown in Fig. 2 is obtained from Ref. [20]. We have obtained the value of the parameter m_1 , with RMS error=0.0043 using the steepest gradient optimization method [35] to solve the least-square problem for the damage model given in Eq. (1). The value is: $m_1 = 4.0065$. Similarly, we have obtained the optimized values of the parameters q , m_1 , and m_2 RMS error=0.00018 for composites using the damage model given in Eq. (2). The values are: $q = 0.6982$, $m_1 = 0.3399$,

Table 1
Rotor properties

Number of blades	4
Radius (m)	4.94
Hover tip speed (m/s)	198.13
m_0 , kg/m	6.46
$EI_y/m_0\Omega^2 R^4$	0.021
$EI_z/m_0\Omega^2 R^4$	0.0201
$GJ/m_0\Omega^2 R^4$	0.007688

Table 2
Baseline frequencies for first 11 modes

Mode no.	Mode	Frequency/ Ω	Frequency (Hz)
1	First lag	0.74	4.72
2	First flap	1.14	7.28
3	Second flap	3.51	22.41
4	Second lag	4.44	28.34
5	First elastic twist	4.55	29.05
6	Third flap	7.99	51.01
7	First axial	11.05	70.54
8	Third lag	11.30	72.14
9	Second elastic twist	13.48	86.06
10	Fourth flap	14.42	92.06
11	Fourth lag	21.46	137.0

$m_2 = 9.99$. Therefore, for homogenous material, the model is

$$D = \left(\frac{n}{N}\right)^{4.0065} \tag{12}$$

and for composite materials

$$D = 0.6982\left(\frac{n}{N}\right)^{0.3399} + (1 - 0.6982)\left(\frac{n}{N}\right)^{9.99} \tag{13}$$

5.1. Frequency variation

Fig. 4 shows the change in frequency with cycle ratio for homogenous material. We see in Fig. 4 that for homogenous material the change in frequencies with cycle ratio is very less for at least half the total number of cycles ($n/N \approx 0.5$). In the next stage, there is a gradual decrease in frequency with cycle ratio. Finally, we see a rapid decrease in frequencies with time for the rest of the life of the blade. In Fig. 5 we can see that, for composite material, the frequencies decrease rapidly for

the first few cycles. In the next stage, the frequencies decrease slowly and steadily with time. Finally, the frequencies decrease rapidly during the last stage before the failure occurs.

5.2. Frequency delta model

By using a linear transformation of variables, a mathematical model can be developed for the behavior of rotating frequency with time. The difference between the frequency of the damaged and undamaged blade is used as the system indicator for damage and is referred to as a “health residual” and is positive for structural damage because the reduction in stiffness for a damaged blade decreases the frequency. Here, the $\Delta\bar{\omega}$ is defined as $\Delta\bar{\omega} = \omega^{(d)} - \omega^{(u)}$ and is measured in Hertz. The measurement delta is expressed as a percentage change

$$\Delta\omega = 100 \frac{\omega^{(d)} - \omega^{(u)}}{\omega^{(u)}}. \quad (14)$$

According to Gertler [36], a key task in fault detection is residual generation. Residuals are quantities which are nominally zero. However, they become nonzero due to faults (and also due to disturbances, noise and modeling error). Residuals are generated from the monitored plant. Using frequencies, $\Delta\bar{\omega}$ or $\Delta\omega$ can be used as residual generators. A schematic representation of the residual generator is given in Fig. 6. Gertler [36] mentions that because of the presence of noise and modeling errors, residuals need to be threshold tested. Such a threshold can be obtained experimentally or through numerical simulators. Any threshold involves a trade-off between false alarms and missed detections. A scalar residual can be threshold tested as follows:

$$\begin{aligned} \text{if } r(t) < T & \text{ then no faults} \\ & \geq T \text{ then fault.} \end{aligned}$$

A good strategy is to declare a fault based on results at several discrete time points. A similar test for a vector residual can be performed using $\|r(t)\|$.

Figs. 7 and 8 illustrate the frequency delta variation with time. The variation in frequency delta pattern is almost similar to the damage growth rate pattern that we can see from Fig. 2. Thus, by the transformation in Eq. (14), the frequency delta variations can be expressed as curves that are similar to Fig. 2. Towards the region of high damage, the frequencies show change of about 10–30%. According to Friswell [37], frequency measurements have a resolution of about 0.1%. Therefore, from Figs. 7 and 8 there is substantial change in frequencies at high damage levels and we can use the evolution of modal frequency as a useful damage indicator. The first lag and torsion mode frequencies show significant change with the lag mode being sensitive to location of damage. At 90% life point, the percent frequency change for the homogenous material is shown in Table 3 and for composite material in Table 4. These frequency changes can be used to define thresholds beyond which it is dangerous to operate the rotor. In general, it is recommended practice to either threshold individual components of the damage indicator $\Delta\omega_i$ or a norm $\|\Delta\omega\|$. For the homogenous material in Table 3, the 4th lag and flap and the first torsion mode show measurable changes for all three damage locations. Thus a rule could be defined as

IF $\Delta\omega(4\text{th lag}) > 4.13\%$ AND $\Delta\omega(4\text{th flap}) > 3.66\%$ AND $\Delta\omega(1\text{st torsion}) > 3.81\%$,
THEN DAMAGE APPROACHES LIFE LIMIT.

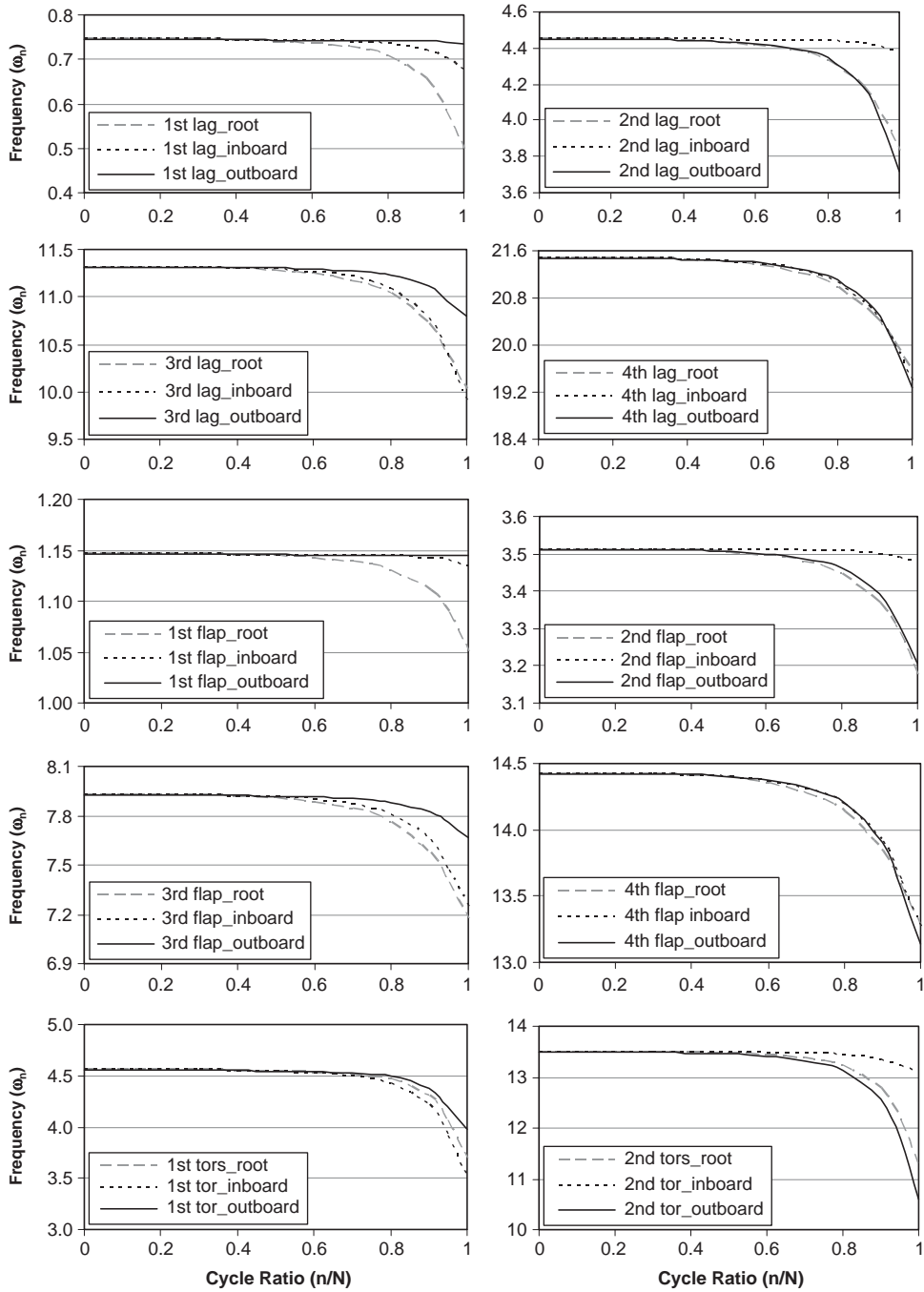


Fig. 4. Frequency variation for homogenous material with cycle ratio.

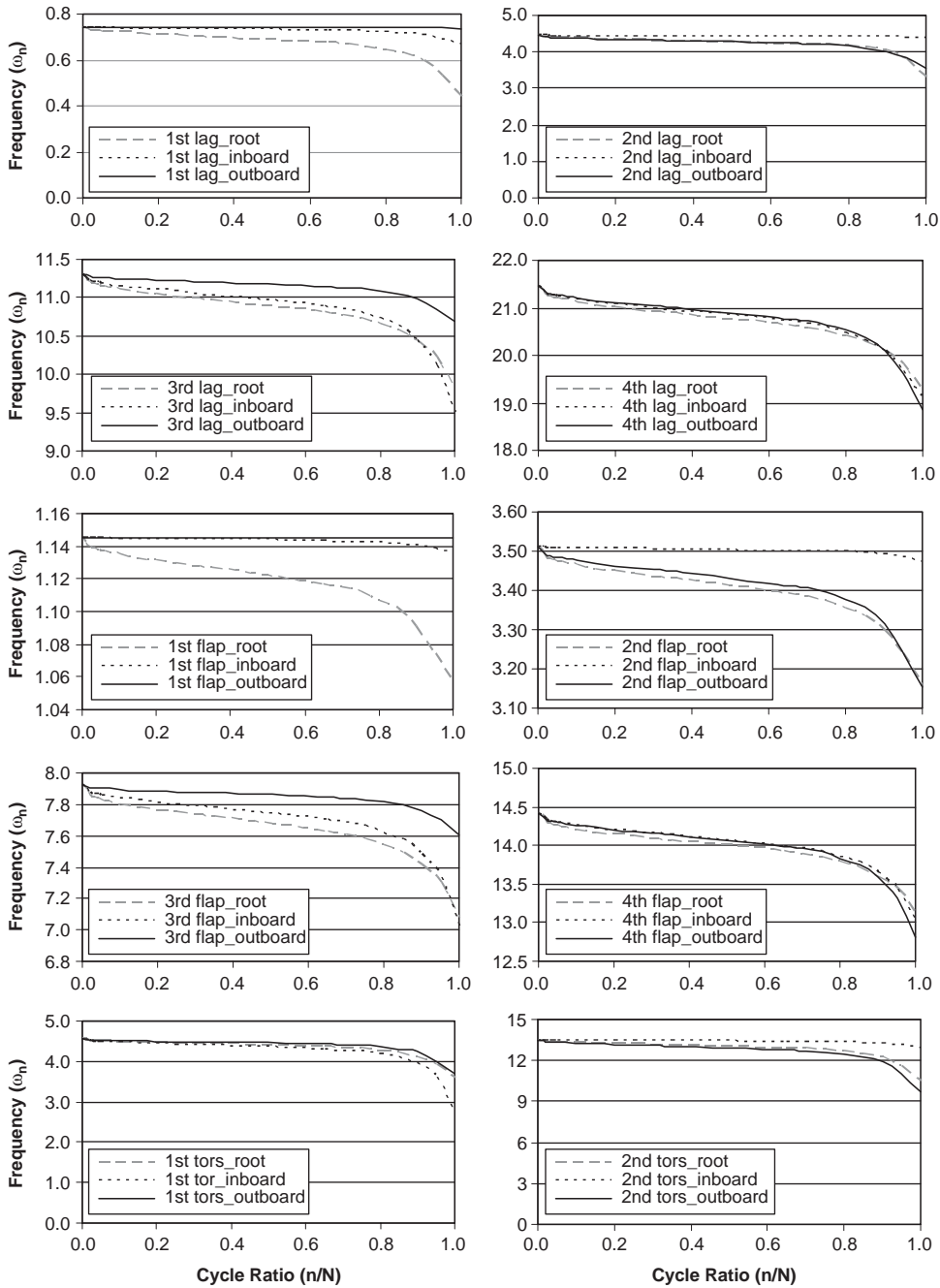


Fig. 5. Frequency variation for composite material with cycle ratio.

Here we have used the minimum change in frequencies to establish a threshold. Such a selection may lead to some false alarms. If we select the maximum change in the frequencies to establish a threshold, more missed alarms will occur. In general, threshold selection involves a tradeoff

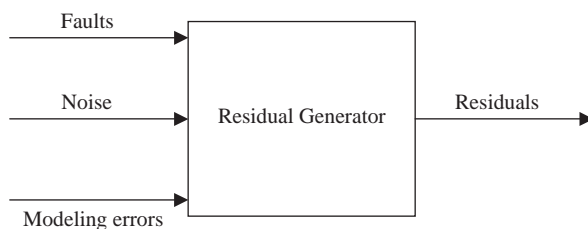


Fig. 6. Schematic representation of residual generator.

between false alarms and missed alarms [36]. The selection of the minimum for thresholding is a conservative choice and minimizes missed alarms. For composite material, the 4th flap, lag and 2nd torsion show change for all the damage locations considered. A rule for damage in this case could be given as

IF $\Delta\omega(4\text{th lag}) > 6.76\%$ AND $\Delta\omega(4\text{th flap}) > 7.39\%$ AND $\Delta\omega(2\text{nd torsion}) > 7.99\%$,
 THEN DAMAGE APPROACHES LIFE LIMIT.

In addition, it is possible to define a diagnostic chart using these results. Let us replace the numerical values of $\Delta\bar{\omega}$ using the following linguistic definition: $0 < \Delta\omega < 2.5\%$, small(S); $2.5 < \Delta\omega < 5\%$, Medium (M); $5 < \Delta\omega < 7.5\%$, Medium High (MH); $7.5 < \Delta\omega < 10\%$, High (H); and $\Delta\omega > 7.5\%$, Very High (VH). Then Tables 3 and 4 can be expressed as Tables 5 and 6, which represent a knowledge base for an expert system and is a diagnostic chart.

From Figs. 7 and 8, it is clear that the frequency delta variations follow a form that is similar to the damage growth models in Fig. 2. As an example, we consider the curve for 3rd lag mode frequency delta for inboard damage and fit the expressions in Eq. (1) for homogenous material and Eq. (2) for composite material.

For the 3rd lag $\Delta\omega$, using the curves shown in Figs. 9 and 10, we have obtained the optimized value of the parameter for homogenous material $m_1 = 5.1483$ and for composite material $q = 0.3349$, $m_1 = 0.4341$, $m_2 = 11.0069$, with RMS error = 0.00052 and RMS error = 0.0046, respectively, for homogenous and composite material by using the steepest gradient and DFP method [35] to solve the least-square problem for best curve fit. For homogenous material, the model is

$$\Delta\bar{\omega} = \left(\frac{n}{N}\right)^{5.1483} \tag{15}$$

and for composite material

$$\Delta\bar{\omega} = 0.3349\left(\frac{n}{N}\right)^{0.4341} + (1 - 0.3349)\left(\frac{n}{N}\right)^{11.0069} . \tag{16}$$

The above results show that there exists a clear relationship between accumulation of damage in the rotor blade and rotating frequencies. Therefore, if we can find out the frequencies at a certain time with the help of some permanently installed sensors on the rotor blade, we can calculate the damage at that particular time and we can know the condition of the helicopter blade and its remaining life at that instant of time. This could be done by tests of the type described in Ref. [13]

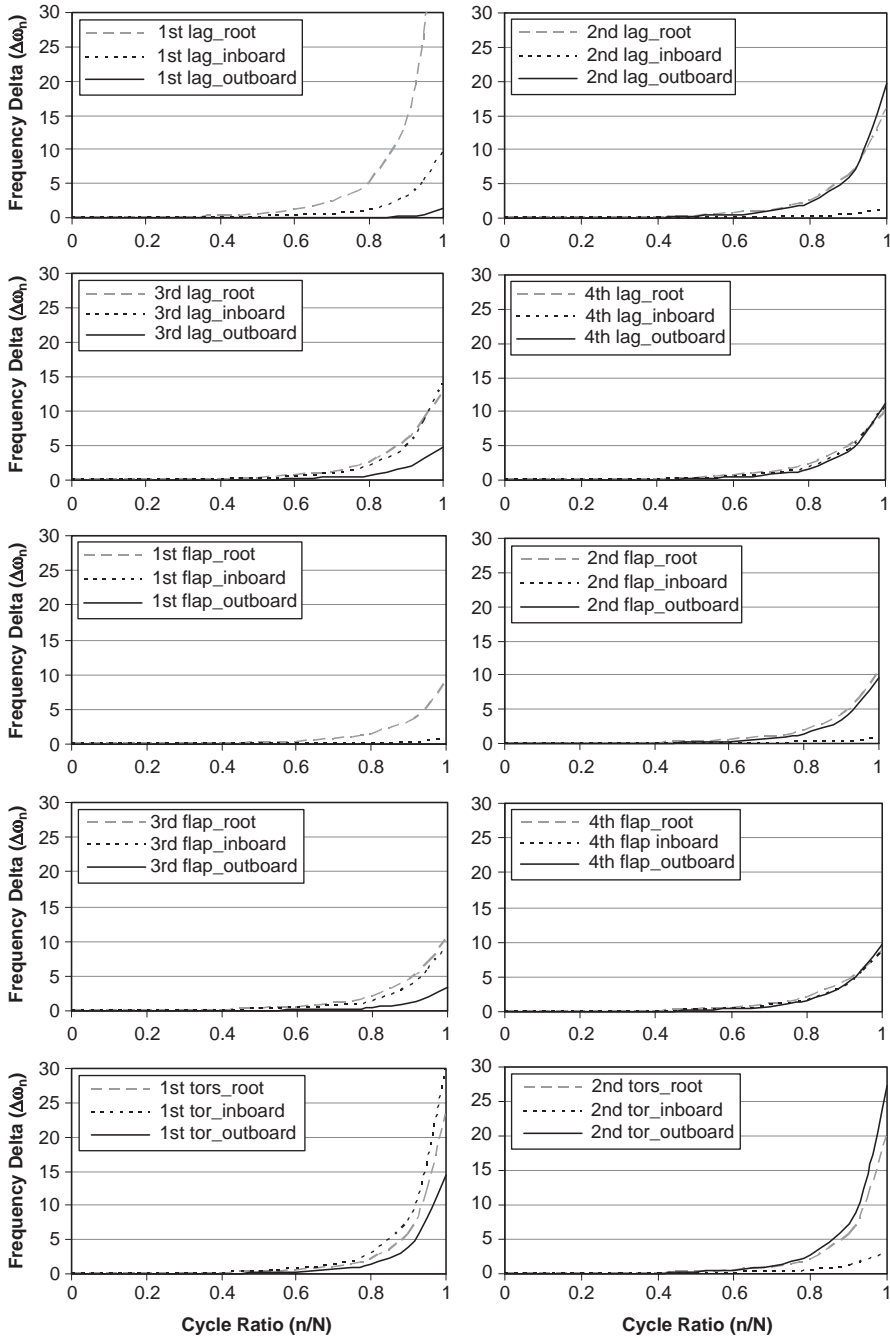


Fig. 7. Frequency delta variation for homogenous material with cycle ratio.

and Fig. 1. after certain specified time intervals. So the rotating frequencies can be considered as virtual sensors of damage. A virtual sensor uses model-based information to ‘measure’ a difficult-to-measure variable. For example, the damage D is difficult to measure directly but can be found

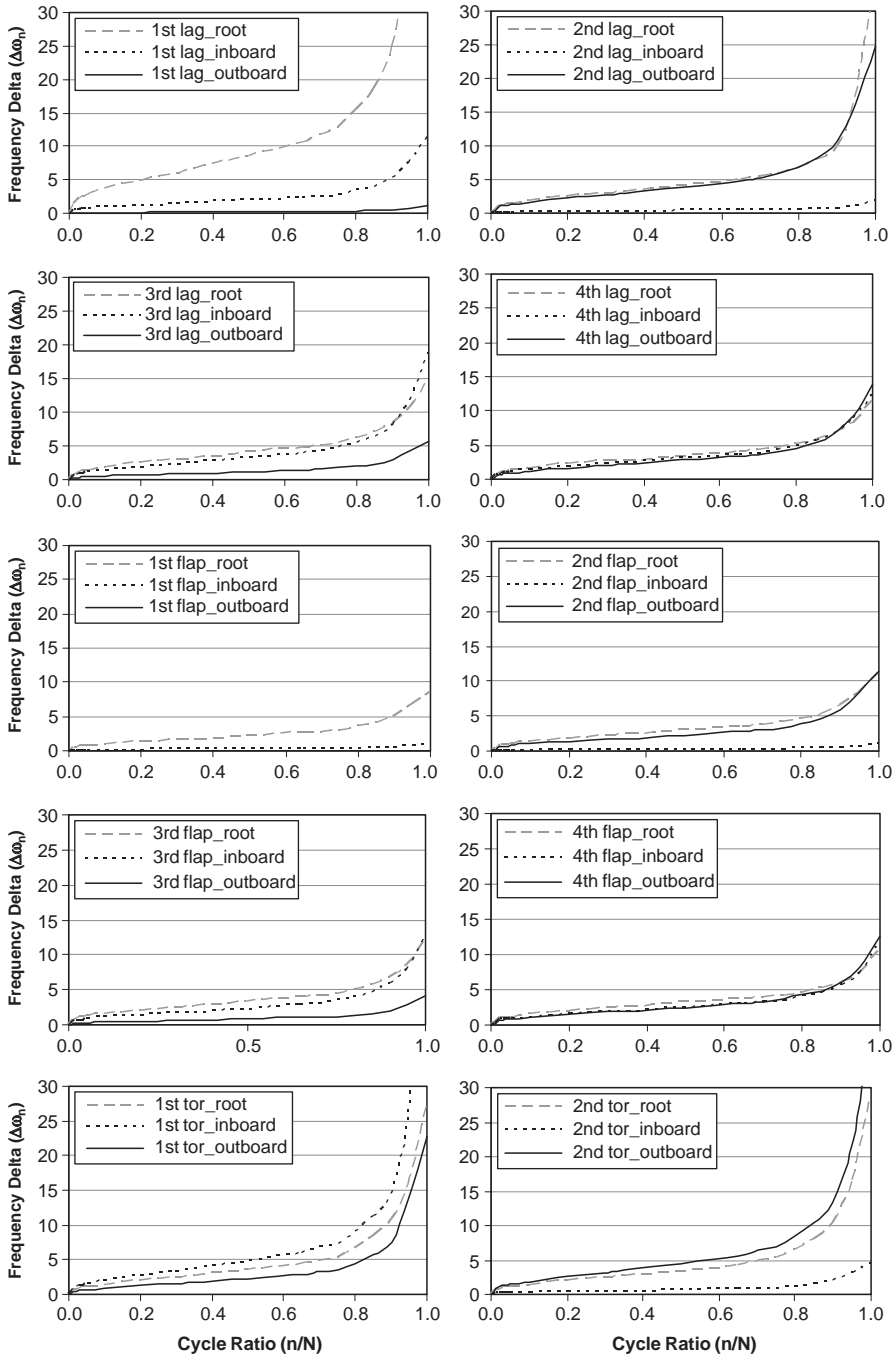


Fig. 8. Frequency delta variation for composite material with cycle ratio.

Table 3
Frequency delta for homogenous material of $n/N = 0.9$ at different damage levels

Modes	Root	Inboard	Outboard
First lag	13.50	2.97	0.28
Second lag	6.11	0.45	6.06
Third lag	5.60	4.87	1.79
Fourth lag	4.76	4.39	4.13
First flap	3.10	0.26	0.01
Second flap	4.19	0.31	3.49
Third flap	4.60	3.51	1.21
Fourth flap	4.22	3.66	3.75
First elastic twist	5.70	7.80	3.82
Second elastic	5.59	1.06	7.34

Table 4
Frequency delta for composite material of $n/N = 0.9$ at different damage levels

Modes	Root	Inboard	Outboard
First lag	24.93	5.16	0.51
Second lag	9.71	0.79	10.69
Third lag	8.39	8.20	3.00
Fourth lag	6.79	6.81	6.76
First flap	4.99	0.43	0.02
Second flap	6.52	0.53	5.94
Third flap	6.88	5.82	2.04
Fourth flap	10.91	14.66	7.39
First elastic twist	10.16	1.89	13.32
Second elastic	11.81	15.89	7.99

Table 5
Frequency delta signature for homogenous material of $n/N = 0.9$ at different damage levels

Modes	Root	Inboard	Outboard
First lag	VH	M	S
Second lag	MH	S	MH
Third lag	MH	M	S
Fourth lag	M	M	M
First flap	M	S	S
Second flap	M	S	M
Third flap	M	M	S
Fourth flap	M	M	M
First elastic twist	MH	H	M
Second elastic	MH	S	MH

Table 6
Frequency delta signature for composite material of $n/N = 0.9$ at different damage levels

Modes	Root	Inboard	Outboard
First lag	VH	MH	S
Second lag	H	S	VH
Third lag	H	H	M
Fourth lag	MH	MH	MH
First flap	M	S	S
Second flap	MH	S	MH
Third flap	MH	MH	S
Fourth flap	VH	VH	MH
First elastic twist	VH	S	VH
Second elastic	VH	VH	H

using Eqs. (12),(13) and (15),(16) once $\Delta\omega$ is known. Similarly, the used-up life (n/N) of the structures can be found from Eqs. (15) and (16) if $\Delta\omega$ is known.

6. Signal processing

A key issue in the design of virtual sensors is their sensitivity to modeling errors and noise [38]. A good strategy to improve detection is by filtering the residuals, usually by low-pass algorithm, to reduce the effect of noise while keeping the features representing the fault. A schematic representation of the filter proposed in Ref. [36] is shown in Fig. 11. The low-pass filter is applied individually to each element of the residual vector. Typically, linear low-pass filters are used. In general, filtering greatly improves fault detection performance. However, long window filters which are more effective in noise removal can result in detection delay because of excessive smoothing [36]. In operational deployment, noise is always present in sensor measurements. Helicopters are also highly noisy and one problem with using higher modes for health monitoring is that they can have relatively higher levels of noise than the lower modes. Another problem is that, besides Gaussian noise, outliers can be present in the measurements. While linear filters which are mostly used for denoising residuals are optimal for Gaussian noise removal, they are not good at removing outliers and also tend to smooth out the sharp changes in the signal which occur before failure. The nature of the signal prior to failure is critical and needs to be preserved while removing noise and outliers. The weighted recursive median filter is a good tool for such signals (given in Eq. (10)). This WRM filter was discussed before. The procedure for proper weight selection of the WRM filter is discussed below. To the best of the author's knowledge, such an optimal WRM filter is developed for the first time.

6.1. Filter weight selection

We consider the 3rd lag mode frequency as our test signal, and use a nine-point weighted symmetric recursive median filter for our study. For symmetric weights, this WRM filter can be

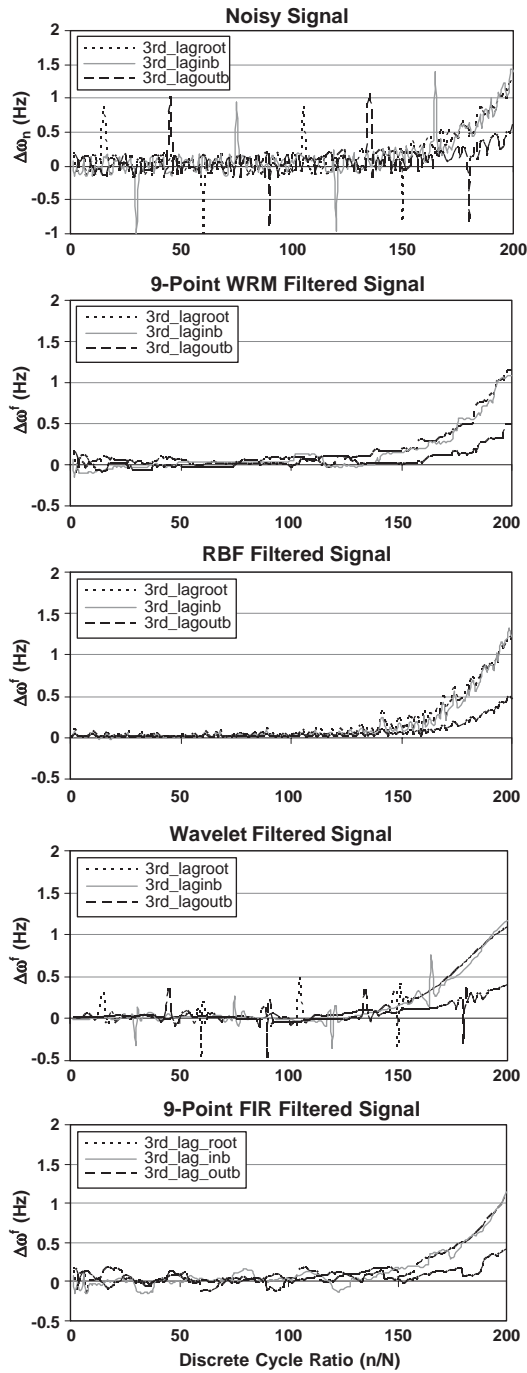


Fig. 9. Noisy test signal for the homogenous material and the effect of WRM, RBF, wavelet and FIR filters on the noisy signal.

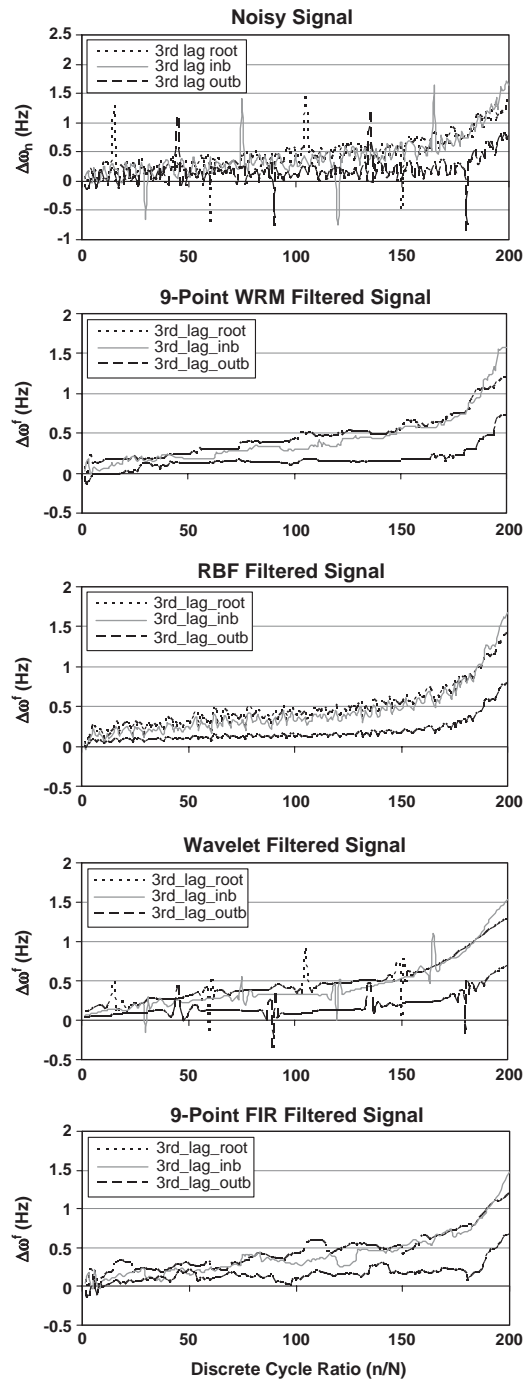


Fig. 10. Noisy test signal for the composite material and the effect of WRM, RBF, wavelet and FIR filters on the noisy signal.

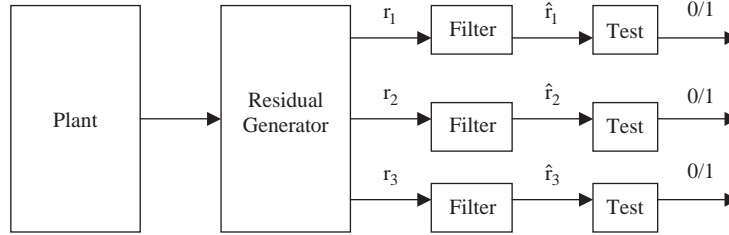


Fig. 11. Schematic representation of residual generator filter.

written as

$$y_n = \text{median}(w_1 \circ y_{n-4}, w_2 \circ y_{n-3}, w_3 \circ x_{n-2}, w_4 \circ x_{n-1}, w_5 \circ x_n, w_4 \circ x_{n+1}, w_3 \circ x_{n+2}, w_2 \circ x_{n+3}, w_1 \circ x_{n+4}). \tag{17}$$

The above filter needs nine points: the current points, four forward points and four backward points. Because it needs four forward points, it has a four-point time delay. To obtain a quantitative idea of the noise reduction, we look at the root mean square error in the signal, which is a measure of the difference between the noisy or filtered and the ideal signal and is given as

$$\text{RMS} = \sqrt{\frac{1}{N} \sum_{i=1}^N (\Delta z_i - \Delta z_i^0)^2}. \tag{18}$$

The RMS is a measure of noise in the signal. Using the RMS definition, we can create a measure for noise reduction for a noisy signal after filtering as

$$N_R = 100 \frac{\text{RMS}^{(\text{noisy})} - \text{RMS}^{(\text{filtered})}}{\text{RMS}^{(\text{noisy})}}. \tag{19}$$

For finding the optimal weights for the nine-point filter, 200 samples of noisy data are used. Gaussian noise is added to the signals with standard deviation ranging from $\sigma = 0.05$ to 0.3 . Because the values of the ideal signals range between 0 and 1, this range of standard deviations considered above covers values of signal-to-noise ratios normally found in damage detection applications. For a given standard deviation σ , the filter design problem can be posed as an optimization problem and written as follows:

$$\text{Maximize } N_R(w_1, w_2, w_3)$$

$$\text{subject to } w_i^{\min} \leq w_i \leq w_i^{\max},$$

where the design variables or weights take on integer values. Reasonable values for the weights can be found in the lower integers, so we select the minimum and maximum weights to be 1 and 7, respectively. The problem then becomes a nonlinear integer programming problem (a nonlinear optimization problem with integer design variable), which we solve using genetic algorithms. Genetic algorithms are stochastic optimization methods, which are especially suited for problems with discrete and integer design variables, and global and local minima. For the genetic algorithm [39], we select each weight to be represented by a three-bit binary string. The minimum weight is

thus binary 001, which corresponds to integer 1. The maximum weight is binary 111, which corresponds to integer 7. The three weights therefore form a nine-bit string. We use a starting population of 20 points, crossover probability of 0.80 and mutation probability of 0.20. The maximum number of generations used is 200. The results are selected for the best points obtained in 200 generations. For each case, there are three global minima that give three sets of weights with the same level of RMS-based noise reduction. These minima are $(w_1, w_2, w_3, w_4, w_5) = (1, 1, 1, 1, 2), (2, 2, 2, 2, 4)$ and $(4, 4, 4, 4, 6)$, respectively. The lowest weights are selected for these cases since that creates the recursive median with the least complexity. Note that finding the median involves sorting the signal, so low weights lead to smaller arrays to sort and lower computer time.

The results show that the best weights for the nine-point recursive median filter for the test signal are: $w_1 = 1, w_2 = 1, w_3 = 1$ and $w_4 = 1$ and $w_5 = 2$. The nine-point optimal filter can therefore be written as

$$y_n = \text{median}(y_{n-4}, y_{n-3}, x_{n-2}, x_{n-1}, 2 \circ x_n, x_{n+1}, x_{n+2}, x_{n+3}, x_{n+4}). \tag{20}$$

In the above problem, though we started with filters of odd length (9), we have obtained a filter of even length using the GA. Thus, the nine-point filter with weights (1, 1, 1, 1, 2) has length $(1 + 1 + 1 + 1 + 2 + 1 + 1 + 1 + 1 = 10)$. Most applications of median filters are odd in length because the median of an odd sequence of numbers is defined as the middle value after sorting. For example, the median of five numbers x^0, x^1, x^2, x^3 and x^4 , where $x^4 \geq x^3 \geq x^2 \geq x^1 \geq x^0$ is given as $\tilde{x} = x^2$. For an even sequence, x^0, x^1, x^2 and x^3 , where $x^3 \geq x^2 \geq x^1 \geq x^0$, the four-point median filter is defined as, $\tilde{x} = \frac{1}{2}(x^1 + x^2)$. The performance of this averaging operation means that the output of even-length filters is not limited to one of the input samples, which is the case with odd-length filter. Havlicek [40] et al. has presented examples where even-length median filters offer improved results compared to odd length filters. They suggested that even-length filters should be considered for filter design.

6.2. Neural network training

We also use the RBF neural network for denoising the test signal. For determining the RBF unit centers, we have used a ‘K-means’ clustering algorithm. The ‘K-means’ clustering algorithm finds a set of clusters, each with centers from the given training data. The cluster centers become the centers of the RBF units. The number of clusters, $H = 20$, is a design parameter and determines the number of RBF units, i.e. nodes, in the hidden layer. When the RBF centers have been established, the widths of each RBF can be calculated. The width of any RBF distance to the nearest $p = 5$ RBF units, where p is a design parameter for the RBFN, for unit i is given by

$$\sigma_i = \sqrt{\left[\frac{1}{p} \sum_{j=1}^p \sum_{k=1}^r (x_{ki} - x_{kj})^2 \right]}, \tag{21}$$

where x_{ki} and x_{kj} are the k th entries of the centers of the i th and j th hidden units. This section of the algorithm generates the necessary centers and widths for the RBFs. When the centers and widths of the RBF units have been chosen, then the $N = 200$ training samples are processed through the hidden nodes to generate an $H \times N$ matrix, called A . Let T be the $M \times N$ desired output matrix for the training patterns and $M = 200$ be the number of output nodes. The

objective is to find the weights that minimize the error between the actual output and the desired output of the network. Essentially, we are trying to minimize the objective (cost) function

$$\|T - WA\|, \quad (22)$$

where W is the $M \times H$ matrix of weights on the connections between the hidden and output nodes of the network. We train the RBF network with added Gaussian noise $\sigma = 0.05-0.1$.

6.3. Wavelet thresholding

Most noise removal methods actually require knowledge of the noise content in the time series. With wavelet denoising, it is not necessary to know which part of the signal is white noise. The WT is applied to the signal and all coefficients below a certain size are discarded [33]. This technique makes use of the fact that some of the decomposed wavelet coefficients correspond to signal averages and others are associated with details on the original signal. If the smaller details are eliminated from the signal decomposition, the original signal can be extracted from the remaining coefficients and the main signal characteristic will remain intact because an orthogonal wavelet transform compresses the ‘energy’ of the signal into a few large components. The white noise is very disordered and hence it is scattered throughout the transform in small coefficients.

6.4. Signal processing results

Figs. 9 and 10 show results for the 3rd lag mode $\Delta\bar{\omega}$ for the nine-point WRM filter discussed above and the RBF and nine-point FIR filter for homogenous and composite material, respectively. In these signals, Gaussian noise is added with $\sigma = 0.1$ Hz and outliers are added to simulate a real rotor signal. Outliers can be mistaken for a trend shift by diagnostic algorithm and their removal is useful before performing fault detection and isolation functions. It is clear from Figs. 9 and 10 that using WRM and RBF filter, visual quality of the signal is considerably improved and there is considerable noise reduction as compared to linear filters. The linear filter used here is the nine-point FIR moving average filter. The improvement in the visual quality of the signal is a feature that has been observed using nonlinear filtering algorithms. Alliney [41] notes that the resulting signals after nonlinear filtering appear satisfactory from the visual point of view and mentions that this may be due to the nonlinear filtering behavior of the human visual system.

The results in Figs. 9 and 10 show the visual effect of applying the filters on noisy signals. To obtain quantitative values of noise reduction, 200 samples of noisy data are taken with $\sigma = 0.05-0.1$ and the noise reduction calculated using Eq. (19). Tables 7 and 8 show noise reduction obtained using the 9-point WRM filter. We observe from Table 7 that, using this nine-point WRM filter, we obtain a considerable noise reduction in the 3rd lag mode (inboard) $\Delta\bar{\omega}$ signal ranging from 70% to 77% in the presence of outlier and 60% to 64% in the absence outliers in the signal for homogenous materials is obtained. For composite material, a noise reduction of 70–75% in the presence of outliers and 55–63% in the absence of outliers in the signal is obtained as shown in Table 8.

Table 7

Noise reduction for test signal with optimal nine-point WRM filter for homogenous material

Noise level, σ	Noise reduction (%) in the absence of outlier	Noise reduction (%) in the presence of outlier
0.05	59.79	76.81
0.06	61.00	74.71
0.08	62.76	71.86
0.10	64.04	70.24
Average	61.89	73.41

Table 8

Noise reduction for test signal with optimal nine-point WRM filter for composite material

Noise level, σ	Noise reduction (%) in the absence of outlier	Noise reduction (%) in the presence of outlier
0.05	55.05	74.51
0.06	57.22	72.68
0.08	60.36	70.43
0.10	62.50	69.30
Average	58.58	71.73

Once the neural network has been trained, it is tested with the simulated signals for different noise levels, $\sigma = 0.05-0.1$. Tables 9 and 10 show the noise reduction obtained using the RBFN: considerable noise reduction of 36–69% for homogenous material and 32–68% for composite material in the absence of outlier in the signal at different noise levels. When the outliers are present in the signal, we get a noise reduction of 64–74% for homogenous material and 58–74% for composite material at different noise levels.

Several wavelets were used for signal denoising. While no one wavelet seemed to consistently give better results than the other, there are some recommendations that can be made, the Daubechis 5, 6, 8 wavelets seemed to produce slightly better results in terms of noise removal. The lower order wavelet did not perform as well as their higher order counterparts due to their properties such as support length, regularity, and number of vanishing moments. The important fact to note here is that wavelets are not very good for discarding the outliers present in the signal. Krim and Schick [42] mention in their work that wavelet denoising is sensitive to outliers, i.e., to noise distributions whose tails are heavier than the Gaussian distribution. Therefore, the presence of outlier in the signal deteriorates the denoising efficiency. The Wavelet filter results in Tables 11 and 12 show better noise reduction than the WRM and the RBF filter in the absence of outliers, but lower noise reduction than WRM and RBF in the presence of outliers in the signal. We can see the performance of the wavelet filter visually in Figs. 9 and 10.

Table 9
Noise reduction for test signal with RBF for homogenous material

Noise level, σ	Noise reduction (%) in the absence of outlier	Noise reduction (%) in the presence of outlier
0.05	36.07	64.25
0.06	47.37	66.89
0.08	60.51	69.56
0.10	69.07	73.73
Average	53.25	68.61

Table 10
Noise reduction for test signal with RBF for composite material

Noise level, σ	Noise reduction (%) in the absence of outlier	Noise reduction (%) in the presence of outlier
0.05	31.99	30.62
0.06	44.52	33.65
0.08	60.03	39.47
0.10	67.96	73.68
Average	51.13	66.04

From Tables 8–10, it is clear that the WRM filter performs better than the RBF at lower noise levels ($\sigma = 0.05, 0.06$ and 0.08), but the RBF performs better at $\sigma = 0.10$. The FIR results in Tables 13 and 14 show lower noise reduction than the WRM and the RBF filter. Finally, Tables 15–18 give the noise reduction obtained by the 3rd lag frequency for noise level $\sigma = 0.10$. In these tables, all the three damage locations are considered. Again, it is clear that the WRM and RBF filters result in considerable noise reduction. For homogenous material, the noise reductions using WRM, RBF, wavelet and FIR filters are about 70%, 74%, 56% and 54%, respectively. For the composite material, the average noise reductions using WRM, RBF, wavelet and FIR filters are 76%, 75%, 56% and 59%, respectively. Therefore, we can conclude that the WRM and RBF filters are competitive filters for denoising of damage indicator time series containing sharp trend shifts and noise. The WRM filter is relatively simple to design and use and is recommended for health-monitoring operations.

Finally, we note several assumptions made in this study. Biased noise which can result from variability in the dynamic characteristic of the rotor and vehicle due to environmental conditions is not considered. The study considers a constant load where actual loads have non-stationary components which can cause unusual damage growth due to changes in the distribution of residual stresses around the cracked zone. Nonlinear plastic deformations which can be important for both homogenous and heterogeneous materials especially prior to failure are not considered. These issues are subjects of future work.

Table 11
Noise reduction for test signal with Wavelet filter homogenous material

Noise level, σ	Noise reduction (%) in the absence of outlier	Noise reduction (%) in the presence of outlier
0.05	74.21	32.77
0.06	74.95	37.89
0.08	75.58	47.58
0.10	76.16	55.46
Average	74.97	43.42

Table 12
Noise reduction for test signal with Wavelet filter composite material

Noise level, σ	Noise reduction (%) in the absence of outlier	Noise reduction (%) in the presence of outlier
0.05	64.41	31.96
0.06	66.02	37.10
0.08	69.94	46.75
0.10	72.11	54.68
Average	68.12	42.62

Table 13
Noise reduction for test signal with FIR filter homogenous material

Noise level, σ	Noise reduction (%) in the absence of outlier	Noise reduction (%) in the presence of outlier
0.05	15.17	46.53
0.06	25.71	47.82
0.08	38.26	50.30
0.10	45.29	52.47
Average	31.16	49.28

Table 14
Noise reduction for test signal with FIR filter composite material

Noise level, σ	Noise reduction (%) in the absence of outlier	Noise reduction (%) in the presence of outlier
0.05	25.02	52.33
0.06	33.91	53.28
0.08	44.34	55.10
0.10	50.06	56.64
Average	38.33	54.34

Table 15

Percent noise reduction in RMS error for test signals for WRM filter in the presence of outliers in the signal and at a noise level of $\sigma = 0.1$

Frequency delta $\Delta\omega$	Noise reduction (%) for homogenous material with outlier	Noise reduction (%) for composite material
3rd lag root	70.24	69.30
3rd lag inboard	71.18	78.63
3rd lag outboard	73.22	81.03
Average	71.54	76.32

Table 16

Percent noise reduction in RMS error for test signals for optimal RBF filter in the presence of outliers in the signal and at a noise level of $\sigma = 0.1$

Frequency delta $\Delta\omega$	Noise reduction (%) for homogenous material with outlier	Noise reduction (%) for composite material
3rd lag root	73.73	73.68
3rd lag inboard	73.31	73.46
3rd lag outboard	75.49	78.59
Average	74.18	75.20

Table 17

Percent noise reduction in RMS error for test signals for wavelet filter in the presence of outliers in the signal and at a noise level of $\sigma = 0.1$

Frequency delta $\Delta\omega$	Noise reduction (%) for homogenous material with outlier	Noise reduction (%) for composite material
3rd lag root	55.46	54.68
3rd lag inboard	56.73	55.92
3rd lag outboard	56.11	56.25
Average	56.10	55.61

7. Conclusions

A qualitative study of the effect of damage growth on rotor system modal frequencies and evaluation of their feasibility for monitoring of fatigue damage and blade life is done in this study. The following conclusions are made:

1. By using change of frequency between the damaged and undamaged blade as a damage indicator, it is found that the damage indicator shows an evolution with cycles that can be modeled using functional relationships identical to those used to model the damage.

Table 18

Percent noise reduction in RMS error for test signals for FIR filter in the presence of outliers in the signal and at a noise level of $\sigma = 0.1$

Frequency delta $\Delta\omega$	Noise reduction (%) for homogenous material with outlier	Noise reduction (%) for composite material
3rd lag root	52.47	56.64
3rd lag inboard	51.20	58.89
3rd lag outboard	59.60	60.61
Average	54.42	58.71

2. There is sufficient change in the frequencies to identify the presence of damage in the blade. There is a clear relationship between rotating frequencies and cycles that can be used as a virtual sensor indicating the amount of cumulative damage growth in the structure and the remaining life. Thresholding methods for fault detection are discussed and diagnostic charts for use by knowledge-based systems are proposed.
3. The rotation effect acts to reduce the sensitivity of frequencies to small damage, thereby preventing spurious alarms. This reduction in sensitivity of frequencies of small damage is an advantage since helicopter blades are routinely built to take large quantity of damage.
4. Because actual online data are contaminated with noise and outliers, a powerful signal-processing approach based on an optimally weighted recursive median filter and radial basis function neural network and wavelets is developed in this study. The WRM and RBF filters perform better than the wavelet and FIR moving average filter and can be used to clean data prior to fault detection and isolation. Wavelets are not good at removing outliers from data.
5. The optimum WRM and RBF filters improve the visual quality of the signals by removing outliers and random noise. Thus, they can be used as a preprocessing smoother before displaying condition and health-monitoring data for improved visualization, and result in better human-based diagnostics.

References

- [1] H. Azzam, M.J. Andrews, The use of math dynamic models to aid the development of integrated health and usage monitoring systems, *Proceedings of The Institution of Mechanical Engineers* 206 (G1) (1992).
- [2] J. Alkahe, Y. Oshman, O. Rand, Adaptive estimation methodology for helicopter blade structural damage detection, *Journal of Guidance, Control, and Dynamics* 25 (2002) 1049–1057.
- [3] R. Ganguli, Health monitoring of a helicopter rotor in forward flight using fuzzy logic, *AIAA Journal* 40 (2002) 2373–2382.
- [4] R. Ganguli, I. Chopra, D.J. Haas, Detection of helicopter rotor system simulated faults using neural networks, *Journal of the American Helicopter Society* 42 (2) (1997) 161–171.
- [5] J. Kiddy, D. Pines, Damage detection of main rotor faults using a sensitivity approach, *Proceedings of the Institute of Mechanical Engineers Part I: Journal of Systems & Control in Engineering* 215 (2001) 209–220.
- [6] J. Cattarius, D.J. Inman, Experimental verification of intelligent fault detection in rotor blades, *International Journal of Systems Science* 31 (2000) 1375–1379.

- [7] R. Ganguli, A fuzzy logic system for ground based structural health monitoring of a helicopter rotor using modal data, *Journal of Intelligent Material Systems and Structures* 12 (2001) 397–408.
- [8] G.C. Larsen, A.M. Hansen, O.J.D. Kristensen, Identification of damage to wind turbine blades by modal parameter estimation, Report Riso-R-1334 (EN), Riso National Laboratory, Roskilde, Denmark, 2002.
- [9] K.H. Rew, S. Kim, I. Lee, Y. Park, Real time estimation of multi-modal frequencies for smart structures, *Smart Materials and Structures* 11 (2002) 36–47.
- [10] R. Brinker, L. Zhang, P. Andersen, Modal identification of output-only system using frequency domain decomposition, *Smart Materials and Structures* 10 (2001) 441–445.
- [11] I. Bucher, D.J. Ewins, Modal analysis and testing of rotating structures, *Philosophical Transactions of the Royal Society of London, Series A: Mathematical and Physical Sciences* 359 (2001) 61–96.
- [12] W.K. Wilkie, P.H. Mirick, C.W. Langston, Rotating shake test and modal analysis of a model helicopter rotor blade, NASA Technical Memorandum 4760, ARL Technical Report 1389, June 1997.
- [13] D.E. Adams, M. Nataraju, A nonlinear dynamics system for structural diagnosis and prognosis, *International Journal of Engineering Science* 40 (2002) 1919–1941.
- [14] D. Chelidze, J.P. Cusumano, A dynamical system approach to failure prognosis, *Journal of Vibration and Acoustics* 126 (2004) 2–8.
- [15] A. Fatemi, L. Yang, Cumulative fatigue damage and life prediction theories: a survey of the state of the art for homogeneous materials, *International Journal of Fatigue* 20 (1998) 9–34.
- [16] J. Degrieck, W. Van Paepegem, Fatigue damage modeling of fibre-reinforced composite materials: review, *Applied Mechanics Reviews* 54 (2001) 279–300.
- [17] S. Nicholas, R. Russ, Elevated temperature fatigue behavior of SCS-6/Ti-24Al-11Nb, *Material Science Engineering A* 153 (1992) 514–519.
- [18] S. Subramanian, K.L. Reifsnider, W.W. Stichcomb, A cumulative damage model to predict the fatigue life of composite laminates including the effect of a fibre–matrix interface, *International Journal of Fatigue* 17 (1995) 343–351.
- [19] H.G. Halverson, W.A. Curtin, K.L. Reifsnider, Fatigue life of individual composite specimens based on intrinsic fatigue behavior, *International Journal of Fatigue* 19 (1997) 369–377.
- [20] H. Mao, S. Mahadevan, Fatigue damage modeling of composite materials, *Composite Structures* 58 (2002) 405–410.
- [21] T. C Moon, H.Y. Kim, W. Hwang, Natural frequency reduction model for matrix dominated fatigue damage of composite laminates, *Composite Structures* 62 (2003) 19–26.
- [22] N.E. Bedewi, D.N. Kung, Effect of fatigue loading on the modal properties of composite structures and its utilization for prediction of residual life, *Composite Structures* 37 (1997) 357–371.
- [23] D.H. Hodges, E.H. Dowell, Nonlinear equations of motion for the elastic bending and torsion twisted non-uniform rotor blades, 1974, NASA TN D-7818.
- [24] R.R.K. Reddy, R. Ganguli, Structural damage detection in a helicopter rotor blade using radial basis function neural networks, *Smart Structures and Materials* 12 (2003) 232–241.
- [25] I. Chopra, N. T. Sivaneri, Aeroelastic stability of rotor blades using finite element analysis, 1982, NASA CR 166389.
- [26] J. Lemaitre, *A Course on Damage Mechanics*, Springer, Berlin, 1992.
- [27] I. Shmulevich, E.J. Coyle, The use of recursive median filters for establishing the tonal context of music, *IEEE Workshop on Nonlinear Signal and Image Processing*, Michigan, USA 1997.
- [28] G.R. Arce, J.L. Paredes, Recursive weighted median filter admitting negative weights and their optimization, *IEEE Transactions on Signal Processing* 48 (3) (2000) 768–779.
- [29] L. Yin, M. Yang, M. Gabbouj, Y. Neuvo, Weighted median filters: a tutorial, *IEEE Transactions on Circuits and Systems* 40 (1996) 147–192.
- [30] C.N. So, J.G. Lucas, Neural network classifier and filtering for EEG detection in brain–computer interface device, in: *Second Conference of the Victorian Chapter of the IEEE Engineering in Medicine and Biology Society*, Victoria, Canada, 2001.
- [31] D. Lin, J.E. Dayhoff, P.A. Ligomenides, Trajectory production with the adaptive time-delay neural network, *Neural Networks* 8 (3) (1995) 447–461.

- [32] J. Leonard, M. Kramer, L.H. Unger, Using radial basis functions to approximate a function and its error bounds, *IEEE Transactions on Neural Networks* 3 (1992) 624–627.
- [33] B.B. Hubbard, *The World According to Wavelets*, Peters, Wellesley, 1996.
- [34] R. Ganguli, Optimum design of a helicopter rotor for low vibration using aeroelastic analysis and response surface methods, *Journal of Sound and Vibration* 258 (2) (2002) 327–344.
- [35] A.D. Belegundu, T.R. Chandrapatla, *Optimization Concepts and application in Engineering*, Prentice- Hall, Englewood Cliffs, NJ, 1999.
- [36] J.J. Gertler, *Fault Detection and Diagnosis in Engineering System*, Marcel Dekker, New York, 1998.
- [37] M.I. Friswell, Penny Jet, Is damage detection using vibration measurements practical?, in: *EUROMECH 65 International Workshop: DAMAS 97; Structural Damage Assessment Using Advanced Signal Processing Procedures*, Sheffield, UK, 1997.
- [38] P. Anberton, G.C. Goodwin, Virtual sensor for control applications, *Annual Reviews in Control* 26 (2002) 101–112.
- [39] D.E. Goldberg, Genetic algorithms in search, optimization, and machine learning, The University of Alabama, 1989.
- [40] J.P. Havliceck, G.R. Katz, J.C. McKeeman, Even length median filter in optimal signal processing, *Electronic Letters* 28 (1995) 1258–1260.
- [41] S. Alliney, Recursive median filters of increasing order: a variational approach, *IEEE Transactions on Signal Processing* 44 (1996) 1346–1354.
- [42] H. Krim, I.C. Schick, Minimax description length for signal denoising and optimized representation, *IEEE Transactions on Information Theory* 45 (3) (1999) 898–908.